Analysis of numerical dissipation in entropy-stable schemes for turbulent flows

By S. M. Murman† AND C. Frontin‡

The effect of subgrid-scale (SGS) modeling on entropy production in entropy-stable formulations is examined. The ignorance of typical modeling approaches to stabilization in compressible turbulence simulations leads to degraded performance. An attractive alternative to entropy-stable methods is the use of entropy-conservative schemes with an appropriate SGS model, which also provides stabilization. A straightforward SGS model is developed using the inviscid stabilization term and shown to provide benefits for homogeneous isotropic turbulence and wall-bounded channel flows.

1. Background

Numerical stabilization for computation of the Navier-Stokes equations is a necessary evil. There are insufficient resources, except in some academic cases, to fully resolve the turbulent stresses. This lack of resolution requires some level of numerical damping in order to limit the growth of unstable modes. Many methods provide numerical stabilization, but one important class is entropy-stable (ES) schemes. These mimetic schemes satisfy the Clausius-Duhem inequality, ensuring that the discrete entropy in the computational domain is a monotonically increasing function.

As part of an effort within NASA, we have recently developed a space-time discontinuous-Galerkin (DG) spectral-element solver (Diosady & Murman 2013, 2014, 2015). The solver uses a robust ES implementation and scale-resolving methods in order to accurately predict the separated flow physics. The scale-resolving model is a dynamic extension of the variational multiscale method (VMM) (Hughes *et al.* 1998, 2000). The VMM is a reformulation of the classical large-eddy simulation (LES) method, in which the filtering operation, used to explicitly separate resolved and unresolved scales, is replaced by a Galerkin projection operator. The long-distance triadic interactions involving the unresolved scales are ignored. The unresolved scales are then assumed to interact only with the finest resolved scales, thus ensuring that no energy is removed from the large structures in the flow via a model (Figure 1).

In order to apply the VMM to general complex flows, including those with separation, it is necessary to replace the original fixed-coefficient model of Hughes *et al.* with a mechanism that automatically adapts to the local resolution and flow physics. This was accomplished during the 2014 CTR Summer Program (Murman *et al.* 2014). For the dynamic procedure, we developed a variational analogue to the dynamic procedure of Germano *et al.* (1991) from classical LES.

Three main difficulties emerge when the dynamic VMM model, or any subgrid scale (SGS) model, is applied using an ES scheme. The first difficulty is the additional dissipation supplied by the stabilization. This can be seen in Figure 2, which presents results

† Advanced Supercomputing Division, NASA Ames Research Center
‡ Department of Aeronautics and Astronautics, Massachusetts Institute of Technology

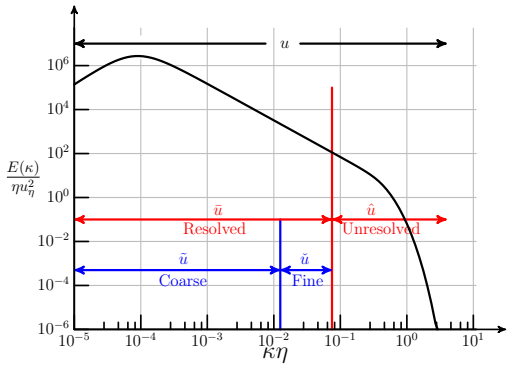

FIGURE 1. *A priori* scale separation for a variational multiscale method following the triple decomposition of Collis (2001).

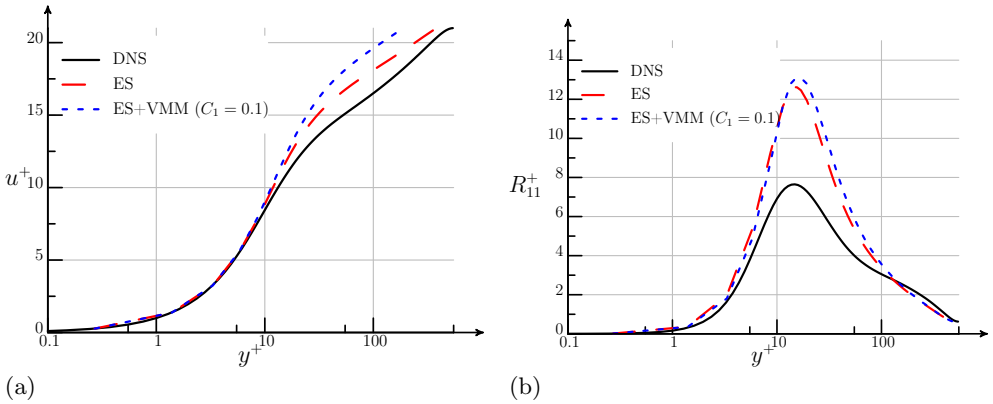

FIGURE 2. Computed velocity profiles and Reynolds stress for channel flow at $Re_\tau = 544$. (a) Mean velocity; (b) R_{11} Reynolds stress. DNS data from Lee & Moser (2015).

for turbulent channel flow simulations at $Re_\tau = 544$ (Murman *et al.* 2016). The VMM results are in worse agreement with the log law than the ES (implicit LES) results are, which only include numerical dissipation from the stabilization terms. In order to achieve positive results with the dynamic VMM, it is necessary to disable the stabilization; i.e. we utilize an entropy-conservative (EC) scheme and expect the dynamic VMM to provide sufficient damping in regions lacking resolution to maintain stability. Unfortunately, this is not always the case, especially in more complex configurations and flows, as the dynamic physical model is not designed to guarantee stabilization.

The second difficulty in applying a dynamic SGS model is that the dynamic procedure used to produce the local SGS model coefficient converges between first order and second order with increasing resolution. We would like any dynamic localization for the SGS model to converge at the same formal rate as the numerical scheme, which is especially true for the high-order methods used in the current work.

Last, the dynamic Germano–Lilly procedure is relatively expensive, requiring multiple evaluations of the nonlinear terms for each step. Further, the procedure is difficult to linearize, impeding the use of implicit schemes, such as in the current space-time solver.

The current work aims to analyze the interaction between the SGS model and the

stabilization terms, specifically in the case of an ES formulation. This analysis is utilized to examine a preliminary SGS model that provides stabilization and converges at the formal rate of the numerical scheme. Examples using homogeneous isotropic turbulence (HIT) and channel flow are provided.

2. Stabilization analysis

The compressible Navier-Stokes equations are written in conservative form as

$$\boldsymbol{u}_{,t} + (\boldsymbol{F}_i^I - \boldsymbol{F}_i^V)_{,i} = 0\,, \tag{2.1}$$

where $\boldsymbol{u} = [\rho, \rho u_j, \rho E]$ is the conservative state vector, and $\boldsymbol{F}_i^I$ and $\boldsymbol{F}_i^V$ are the inviscid and viscous fluxes, respectively. We apply a change of variables, $\boldsymbol{u} = \boldsymbol{u}(\boldsymbol{v})$, where $\boldsymbol{v}$ are the entropy variables,

$$\boldsymbol{v} = \begin{bmatrix} -\frac{s}{\gamma-1} + \frac{\gamma+1}{\gamma-1} - \frac{\rho E}{p} \\ \frac{\rho u_j}{p} \\ -\frac{\rho}{p} \end{bmatrix}, \tag{2.2}$$

with $s = \log(p/\rho^\gamma)$ the entropy. The Navier-Stokes equations may be rewritten as

$$A_0 \boldsymbol{v}_{,t} + A_i \boldsymbol{v}_{,i} - (K_{ij}\boldsymbol{v}_{,j})_{,i} = 0\,, \tag{2.3}$$

with symmetric $A_0 = \boldsymbol{u}_{,\boldsymbol{v}}$, $A_i = \boldsymbol{F}^I_{i,\boldsymbol{u}} A_0 = \boldsymbol{F}^I_{i,\boldsymbol{v}}$, and $K_{ij} = \boldsymbol{F}^V_{i,\boldsymbol{u}_{,j}} A_0 = \boldsymbol{F}^V_{i,\boldsymbol{v}_{,j}}$ (Hughes *et al.* 1986).

Equation (2.3) is discretized on an unstructured spatial domain, Ω, which is partitioned into nonoverlapping elements, κ, while the time is partitioned into time intervals (time slabs), $I^n = [t^n, t^{n+1}]$. Define $\mathcal{V}_h = \left\{\boldsymbol{w}, \boldsymbol{w}|_\kappa \in [\mathcal{P}(\kappa \times I)]^5\right\}$, the space-time finite-element space consisting of piecewise polynomial functions in both space and time on each element. The weak form of the governing equations is given by

$$\sum_\kappa \Big\{ \int_I \int_\kappa - \left(\boldsymbol{w}_{,t}\boldsymbol{u} + \boldsymbol{w}_{,x_i}(\boldsymbol{F}_i^I - \boldsymbol{F}_i^V)\right) + \int_I \int_{\partial\kappa} \boldsymbol{w}(\widehat{\boldsymbol{F}_i^I \boldsymbol{n}_i} - \widehat{\boldsymbol{F}_i^V \boldsymbol{n}_i}) + \int_\kappa \boldsymbol{w}(t_-^{n+1})\boldsymbol{u}(t_-^{n+1}) - \boldsymbol{w}(t_+^n)\boldsymbol{u}(t_-^n) \Big\} = 0\,, \tag{2.4}$$

where the second and third integrals arise owing to the spatial and temporal discontinuity, respectively, of the basis functions. $\widehat{\boldsymbol{F}_i^I \boldsymbol{n}_i}$ and $\widehat{\boldsymbol{F}_i^V \boldsymbol{n}_i}$ denote single-valued numerical flux functions approximating the inviscid and viscous fluxes, respectively, at the spatial boundaries of the elements. In this work, the inviscid flux is examined using several forms, while the viscous flux is computed using the method of Bassi & Rebay (1997). We seek a solution $\boldsymbol{u}(\boldsymbol{v})$, $\boldsymbol{v} \in \mathcal{V}_h$ that satisfies the weak form in Eq. (2.4) for all $\boldsymbol{w} \in \mathcal{V}_h$. The space $\mathcal{V}_h$ is spanned by the tensor product of one-dimensional nodal Lagrange basis functions defined at the Gauss-Legendre points.

The compressible Navier-Stokes equations satisfy the Clausius-Duhem inequality

$$d_{,t}\rho s = \boldsymbol{v}_{,j}^T K_{ij} \boldsymbol{v}_{,i} = \Psi \geq 0\,, \tag{2.5}$$

where the total derivative is given by $d_{,t}\rho s = (\rho s)_{,t} + (\rho u_i s)_{,i} + (q_i/(C_v T))_{,i}$, with q_i representing the heat transfer. Equation (2.5) represents the increase in entropy due to the action of molecular viscosity. As we utilize an ES formulation, we discretely satisfy

the Clausius-Duhem inequality†

$$\Delta_{,t}\rho s = \widehat{\Psi} + \widehat{\Psi}_{\Delta t} + \widehat{\Psi}^I + \widehat{\Psi}^V \geq 0\,, \tag{2.6}$$

where $\widehat{\Psi}$ represents the discrete viscous entropy production, and $\widehat{\Psi}_{\Delta t}$, $\widehat{\Psi}^I$, and $\widehat{\Psi}^V$ are the positive semi-definite numerical stabilization terms due to the temporal, inviscid, and viscous operators, respectively. In the current DG formulation, these stabilization terms are due to the jumps between elements in both space and time (see Gouasmi *et al.* (2018)) for a discussion of the stabilization due to upwinding in time). Further details on the form of these stabilization terms are presented in Appendix A.

The development of physical SGS models for the compressible Navier-Stokes equations has been ignorant of the presence of the stabilization terms in Eq. (2.6) and hence their effect upon the discrete solution. In other words, the typical development of physical models assumes the discrete equations are solved without error. This leads to the difficulty observed in Figure 2.

Here, we seek to develop a subgrid model that is consistent with the numerical stabilization. The dominant stabilization term in Eq. 2.6, at the typical time resolution used in turbulent simulations, is the inviscid term $\widehat{\Psi}^I$. Note that the stabilization due to the upwinding in time is difficult to disable, as the numerical implementation takes advantage of the convenience of upwinding for efficiency. A central question is whether we can choose an EC inviscid flux ($\widehat{\Psi}^I = 0$), as opposed to an ES flux, in combination with a suitable SGS model, and improve over the behavior of the ES formulation without sacrificing robustness.

We examined the performance of the EC inviscid flux for the HIT flow at $Ma_t = 0.1$, $Re_\lambda = 45$. We tested the Ismail & Roe (2009) formulation, the kinetic-energy-preserving formulation of Chandrashekar (2013), and the Tadmor (1987) formulation using a numerical quadrature of 1, 3, and 5 points. At these low-speed conditions, no practical difference between the different flux formulations is present, and in the remainder of this article we use the Ismail & Roe flux.

Typical results for the HIT using the EC and ES numerical schemes at second order and eighth order are presented in the form of the computed energy spectrum in Figure 3. The higher-order simulations resolve more of the physical spectrum, while the lower-order simulations show a mid-wave-number pileup (see Flad & Gassner (2017)). In general there is little difference between the EC and ES simulations. This is the case except at the coarsest resolutions. When a single eighth-order element, or eight degrees of freedom (dof), is used, the EC simulation is unstable, while the ES simulation remains stable. This is indicative of the benefit of the ES approach—robustness in extreme situations. We desire to keep this robustness, but not at the cost of potentially adding unnecessary numerical dissipation due to the stabilization.

3. SGS model

If we assume an ideal EC scheme, i.e. , $\widehat{\Psi}_{\Delta t} = \widehat{\Psi}^I = \widehat{\Psi}^V = 0$, we can derive the entropy condition for an SGS model. We want the evolution of the discrete entropy (Eq. (2.6)) to match the evolution of the true entropy (Eq. (2.5)). Combining these two equations, we have

$$\Delta_{,t}\rho s = \widehat{\Psi} + \left(\Psi - \widehat{\Psi}\right) = \widehat{\Psi} + \widehat{\Psi}_{SGS}\,. \tag{3.1}$$

† While we solve the discrete equations in weak form, we use the strong form here to clarify the discussion.

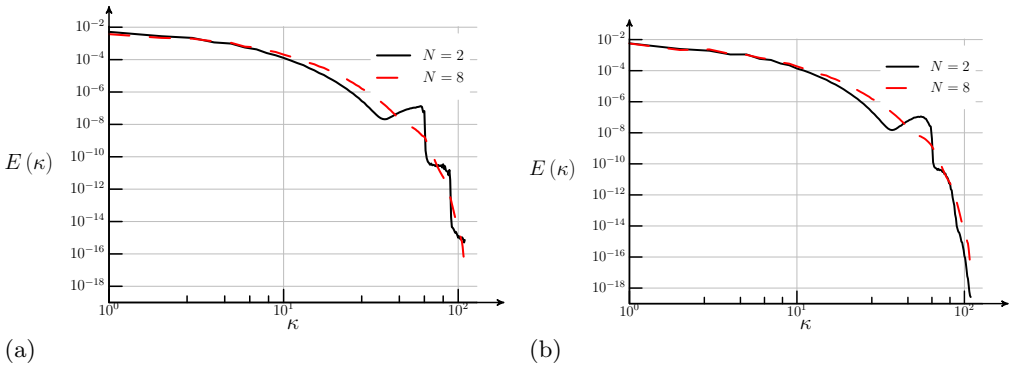

FIGURE 3. Computed energy spectrum for HIT using 128 dof at $Ma_t = 0.1$, $Re_\lambda = 45$. (a) Entropy conservative; (b) entropy stable.

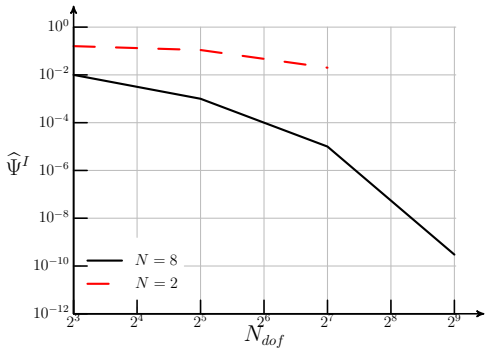

FIGURE 4. Convergence of the inviscid entropy stabilization term, $\widehat{\Psi}^I$, with increasing resolution. $Ma_t = 0.1$, $Re_\lambda = 45$.

It is possible to show that the production of entropy from the SGS model is also positive semi-definite (see Eyink & Drivas 2018). This implies that in an integral sense the SGS model is dissipative (removes energy) and any modeling for effects such as backscatter at a flame front must be accounted for through appropriate limited localization. Note that we derived the effective SGS model in Eq. (3.1) without examination of any nonlinear products or filtering assumptions.

Examining the properties we want for the SGS model, we find that the stabilization terms themselves are attractive. These terms are designed to respond to lack of resolution, are straightforward to compute and linearize, yet converge to zero at the formal rate of the numerical scheme. Figure 4 presents the convergence of $\widehat{\Psi}^I$ with increasing refinement. The asymptotic convergence matches the expected formal rate, with the same holding true for all of the terms in Eq. (2.6).

We formulate an SGS model as

$$\tau = \frac{\widehat{\Psi}^I}{\widehat{\Psi}} K_{ij} \boldsymbol{v}_{,i} = C_{SGS} K_{ij} \boldsymbol{v}_{,i} \tag{3.2}$$

using the ratio of the inviscid entropy stabilization to the viscous entropy production as an SGS coefficient. While this choice is arbitrary, it does provide the following attractive

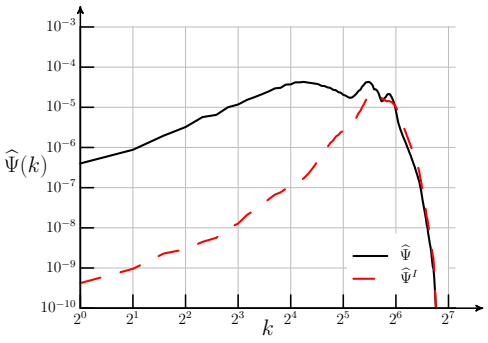

FIGURE 5. Computed energy spectrum for the entropy production terms for the HIT using 128 dof at $Ma_t = 0.1$ and $Re_\lambda = 45$.

dof	N	C_{SGS}
8	2	125
8	8	10.0
32	2	50
32	8	0.2
128	2	5
128	8	0.0025
512	8	1x10^{-7}

Table 1. SGS coefficient $C_{SGS} = \widehat{\Psi}^I/\widehat{\Psi}$ for HIT at $Ma_t = 0.1$ and $Re_\lambda = 45$.

relationship

$$\Delta_{,t}\rho s = \widehat{\Psi} + \boldsymbol{v}_{,j}^T C_{SGS} K_{ij} \boldsymbol{v}_{,i} \Rightarrow \widehat{\Psi} + \widehat{\Psi}^I \,, \tag{3.3}$$

i.e., in an integral sense the SGS model provides the same amount of dissipation as the standard inviscid stabilization term but in a different form.

We can examine this in greater detail by computing the spectrum of the terms $\widehat{\Psi}$ and $\widehat{\Psi}^I$ for a typical HIT simulation (Figure 5). The stabilization term targets damping of the 2Δ modes in the simulation, while the viscous production provides a more broad-spectrum response. In an integral sense, the SGS model is essentially adjusting the magnitude of the viscous dissipation either up or down until it matches the stabilization term.

The SGS model coefficient, $C_{SGS} = \widehat{\Psi}^I/\widehat{\Psi}$, is provided for different resolutions in Table 1. The coefficient provides augmented stabilization at low resolution and approaches zero with increasing resolution. The use of high-order elements greatly reduces the amount of SGS dissipation being added. The EC+SGS scheme, similar to the ES scheme, remains stable at the coarsest resolution for the HIT simulations. The representative energy spectra from this coarse simulation are presented in Figure 6. While there are differences between the approaches, neither displays high-wave-number pileup, which is the goal at these very coarse resolutions.

The behavior in a wall-bounded channel flow at $Re_\tau = 544$ is the final test case. Here, the near-wall spacing is intentionally coarser than typical wall-resolved LES simulations in order to highlight modeling differences. With sufficient resolution, many SGS modeling approaches provide acceptable results, and this mesh resolution is straightforward to

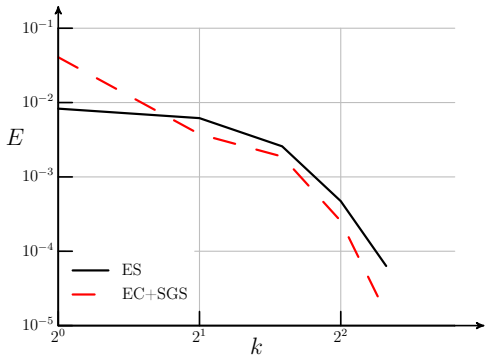

FIGURE 6. Computed energy spectrum for HIT using 8 dof at $Ma_t = 0.1$, $Re_\lambda = 45$.

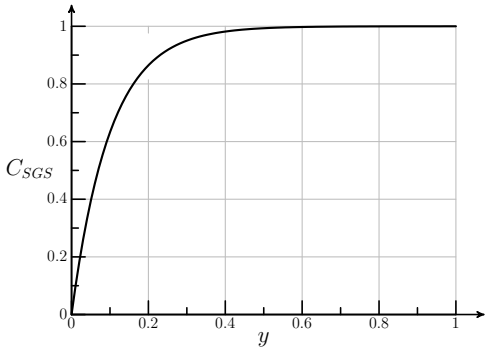

FIGURE 7. Variation of averaged C_{SGS} across the channel $Re_\tau = 544$.

construct for model problems such as the current channel flow. In practical situations, sufficient resolution is not available and is not known *a priori*; hence, we seek to test the behavior under realistic underresolved conditions. The near-wall resolution of the current computational mesh is $\Delta t^+ = 1$, $\Delta x^+ = 100$, $\Delta y^+ = 1$, and $\Delta z^+ = 50$, which is roughly an order of magnitude larger in the streamwise and spanwise directions than the resolution used in the spectral direct numerical simulation (DNS) computations of Lee & Moser (2015). These quoted resolutions represent the average over the wall-adjacent element.

The variation of the averaged SGS coefficient with distance from the wall is presented in Figure 7†. The coefficient decreases to zero within the viscosity-dominated layers near the wall. Note that the typical stabilization is constant across the channel width, as these terms respond to resolution (or lack thereof) and are not aware of the resolved physics. The subsequent simulation results for the mean flow and streamwise Reynolds stress are presented in Figure 8. The EC+SGS approach, unlike the ES approach, does not overly dissipate the turbulence near the wall, unlike the ES approach, yet still provides robust stabilization (Figure 6).

† The variation is projected to a global exponential basis to simplify the numerical implementation for this preliminary experiment.

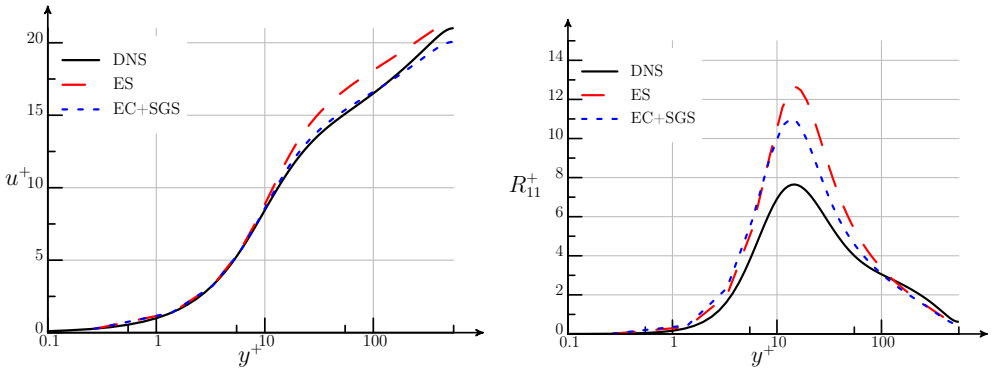

FIGURE 8. Computed velocity profiles and Reynolds stress for channel flow at $Re_\tau = 544$. (a) Mean velocity; (b) R_{11} Reynolds stress. DNS data from Lee & Moser (2015).

Appendix A. Discrete production due to stabilization

The discrete viscous entropy production terms in Eq. (2.6) represent artificial production of entropy due to the stabilization. The various terms are dependent on the choice of spatial and temporal discretization. For the DG formulation used in this paper, upwinding is used for the temporal flux, the method of Ismail & Roe (2009) is used to solve the inviscid flux functions, and the second method of Bassi & Rebay (1997) is used to solve the viscous flux functions.

The entropy produced by the stabilization effect provided by the temporal upwinding term, $\tilde{\Psi}_{\Delta t}$, is a complex but derivable positive, semi-definite function of the jump in state between the end of one temporal element and the beginning of the next. The precise definition of this quantity can be found in the literature (Gouasmi *et al.* 2018).

Ismail and Roe's EC inviscid flux function approximates the inviscid flux at a boundary by

$$\widehat{\mathbf{F}_i^I n_i} = \mathbf{f}_c \,, \tag{A 1}$$

with

$$\mathbf{f}_c = \begin{bmatrix} \hat{\rho}\hat{u} \\ \hat{\rho}\hat{u}^2 + \hat{p}_1 \\ \hat{\rho}\hat{u}\hat{H} \end{bmatrix} \,, \tag{A 2}$$

where the tilde operator, $\widetilde{(\cdot)}$, represents an averaging operation to be defined. These average states can be defined with respect to three variables of interest

$$z_1 = \sqrt{\frac{\rho}{p}} \,, \qquad z_2 = u\sqrt{\frac{\rho}{p}} \,, \qquad z_3 = \sqrt{\rho p} \,. \tag{A 3}$$

Now, if we denote the arithmetic mean of some quantity y by an overbar,

$$\overline{y} = \frac{1}{2}\left(y_L + y_R\right) \tag{A 4}$$

and the logarithmic mean by a superscript ln,

$$y^{\ln} = \frac{y_L - y_R}{\ln(y_L) + \ln(y_R)} \,, \tag{A 5}$$

this gives

$$\begin{aligned}
\hat{\rho} &= \hat{z}_1 z_3^{\ln}\,, & \hat{p}_1 &= \frac{\bar{z}_3}{\bar{z}_1}\,,\\
\hat{p}_2 &= \frac{\gamma+1}{2\gamma}\frac{z_3^{\ln}}{z_1^{\ln}} + \frac{\gamma-1}{2\gamma}\frac{\bar{z}_3}{\bar{z}_1}\,, & \hat{a} &= \left(\frac{\gamma\hat{p}_2}{\hat{\rho}}\right)^{\frac{1}{2}}\,,\\
\hat{H} &= \frac{\hat{a}^2}{\gamma-1} + \frac{1}{2}\hat{a}^2\,.
\end{aligned} \tag{A 6}$$

This EC formulation is formulated such that $\tilde{\Psi}^I = \sum_\kappa \int_I \int_{\partial\Omega} \mathbf{v}\left(\widehat{\mathbf{F}_i^I n_i}\right) = 0$.

Ismail and Roe's ES flux approximates the inviscid flux at a boundary by

$$\widehat{\mathbf{F}_i^I n_i} = \mathbf{f}_c - A[[\mathbf{v}]]\,, \tag{A 7}$$

where A is an symmetric, positive definite matrix form that can be found in the literature, and the jump operator $[[\cdot]]$ is given for a variable y as $[[y]] = y_L n_L + y_R n_R$. This form gives a discrete entropy production term

$$\tilde{\Psi}^I = \sum_\kappa \int_I \int_{\partial\kappa} \mathbf{v} A[[\mathbf{v}]]\,. \tag{A 8}$$

This form can be manipulated to a sum over all the faces to give

$$\tilde{\Psi}^I = \sum_f \int_I \int_f [[\mathbf{v}]] A[[\mathbf{v}]] \geq 0\,. \tag{A 9}$$

The second method of Bassi and Rebay substitutes

$$\int_I \int_{\partial\kappa} \mathbf{w}\left(\mathbf{F}_i^V n_i\right) = \int_I \int_{\partial\kappa} [[\mathbf{w}]] \cdot \{K\nabla_{\text{lift}}\mathbf{v}\} + \{K^T\nabla\mathbf{w}\} \cdot [[\mathbf{v}]] \tag{A 10}$$

into Eq. (2.4), where

$$\mathbf{F}_i^V n_i = K\nabla v \tag{A 11}$$

on $\partial\kappa$. Here, the jump operator is defined as before, the averaging operator $\{\cdot\}$ is given for a given quantity y by $\{y\} = \frac{1}{2}(y_L + y_R)$, and $\nabla_{\text{lift}}(\cdot)$ refers to the gradient computed using the DG lifting operator, which can be found in the literature (Bassi & Rebay 1997).

Choosing $w = v$, we can find

$$\tilde{\Psi}^V = \int_I \int_{\partial\kappa} \mathbf{v}(\mathbf{F}_i^V n_i) = \int_I \int_{\partial\kappa} [[\mathbf{v}]] \cdot \{K\nabla_{\text{lift}}\mathbf{v}\} + \{K^T\nabla\mathbf{v}\} \cdot [[\mathbf{v}]]\,, \tag{A 12}$$

and it can be shown that $\tilde{\Psi}^V \geq 0$.

REFERENCES

Bassi, F. & Rebay, S. 1997 A high-order accurate discontinuous finite element method for the numerical solution of the compressible Navier-Stokes equations. *J. Comput. Phys.* **131**, 267–279.

Chandrashekar, P. 2013 Kinetic energy preserving and entropy stable finite volume schemes for compressible euler and navier-stokes equations. *Commun. Comput. Phys.* **14**, 1252–1286.

Collis, S. S. 2001 Monitoring unresolved scales in multiscale turbulence modeling. *Phys. Fluids* **13**, 1800–1806.

Diosady, L. & Murman, S. 2013 Design of a variational multiscale method for turbulent compressible flows. *AIAA Paper* 2013-2870.

Diosady, L. & Murman, S. 2014 DNS of flows over periodic hills using a discontinuous Galerkin spectral-element method. *AIAA Paper* 2014-2784.

Diosady, L. & Murman, S. 2015 Higher-order methods for compressible turbulent flows using entropy variables. *AIAA Paper* 2015-0294.

Eyink, G. L. & Drivas, T. D. 2018 Cascades and dissipative anomalies in compressible fluid turbulence. *Phys. Rev. X* **8**, 011022.

Flad, D. & Gassner, G. 2017 On the use of kinetic energy preserving DG-schemes for large eddy simulation. *J. Comput. Phys.* **350**, 782–795.

Germano, M., Piomelli, U., Moin, P. & Cabot, W. H. 1991 A dynamic subgrid-scale eddy viscosity model. *Phys. Fluids A* **3**, 1760–1765.

Gouasmi, A., Murman, S.M., & Duraisamy, K. 2018 On entropy stable temporal fluxes. To Appear.

Hughes, T. J., Mazzei, L. & Jansen, K. E. 2000 Large eddy simulation and the variational multiscale method. *Comput. Vis. Sci.* **3**, 47–59.

Hughes, T. J. R., Feijoo, G. R., Mazzei, L. & Quincy, J.-B. 1998 The variational multiscale method–a paradigm for computational mechanics. *Comput. Method. Appl. M.* **166**, 3–24.

Hughes, T. J. R., Franca, L. & Mallet, M. 1986 A new finite element formulation for computational fluid dynamics: I. Symmetric forms of the compressible Euler and Navier-Stokes equations and the second law of thermodynamics. *Comput. Method. Appl. M.* **54**, 223–234.

Ismail, F. & Roe, P. L. 2009 Affordable, entropy-consistent Euler flux functions II: entropy production at shocks. *J. Comput. Phys.* **228**, 5410–5436.

Lee, M. & Moser, R. D. 2015 Direct numerical simulation of turbulent channel flow up to $Re_\tau \approx 5200$. *J. Fluid Mech.* **774**, 395–415.

Murman, S. M., Diosady, L. & Garai, A. 2014 Development of dynamic sub-grid models for variational multiscale methods. *Proceedings of the Summer Program*, Center for Turbulence Research, Stanford University, pp. 397–405.

Murman, S. M., Diosady, L. T., Garai, A., & Ceze, M. 2016 A space-time discontinuous-Galerkin approach for separated flows. *AIAA Paper* 2016-1059.

Tadmor, E. 1987 The numerical viscosity of entropy stable schemes for systems of conservation laws. I. *Math. Comput.* **49**, 91–91.